Gliding basal cell migration of the urothelium during wound healing.

Takeshi Sano[1,2], Takashi Kobayashi[2], Osamu Ogawa[2], Michiyuki Matsuda[1]

[1]*Department of Pathology and Biology of Diseases, Graduate School of Medicine, Kyoto University, Kyoto, Japan*

[2]*Department of Urology, Graduate School of Medicine, Kyoto University, Kyoto, Japan*

Running title: Gliding cell migration of the urothelium

Keywords: Collective cell migration; wound healing; ERK MAP kinase; intravital microscopy

Abbreviations: ERK, extracellular signal-regulated kinase; FRET, Förster resonance energy transfer; TPEM, two-photon excitation microscopy; MEK, MAPK/ERK kinase.

Manuscript: 21 pages, 5 figures, one supplemental Figure and four supplemental video files.

Disclosures: None declared.

Funding: This work was supported by JSPS KAKENHI Grant Numbers 15H02397, 15H05949, 16H06280, CREST JPMJCR1654, and the Nakatani Foundation (MM), and Grant-in-Aid for Young Scientists (A) #25713055 (TK).

Corresponding author:

Michiyuki Matsuda

Department of Pathology and Biology of Diseases, Graduate School of Medicine, Kyoto University, Kyoto, Japan

Yoshida-konoe-cho, Sakyo-ku, Kyoto 606-8501, Japan

Telephone number: +81-75-753-4421

Fax number: +81-75-753-4655

Email address: matsuda.michiyuki.2c@kyoto-u.ac.jp

Abstract

Collective cell migration during wound healing has been extensively studied in the epidermis. However, it remains unknown whether the urothelium repairs wounds in a manner similar to the epidermis. By *in vivo* two-photon excitation microscopy of transgenic mice that express fluorescent biosensors, we studied the collective cell migration of the urothelium in comparison with that of the epidermis. *In vivo* time-lapse imaging revealed that, even in the absence of a wound, urothelial cells continuously moved and sometimes glided as a sheet over the underlying lamina propria. Upon abrasion of the epithelium, the migration speed of each epidermal cell was inversely correlated with the distance to the wound edge. Repetitive activation waves of extracellular signal-regulated kinase (ERK) were generated at and propagated away from the wound edge. In stark contrast, urothelial cells glided as a large sheet over the lamina propria without any ERK activation waves. Accordingly, the MAPK/ERK kinase inhibitor PD0325901 decreased the migration velocity of the epidermis but not the urothelium. Interestingly, the tyrosine kinase inhibitor dasatinib inhibited migration of the urothelium as well as the epidermis, suggesting that the gliding migration of the urothelium is an active, not a passive, migration. In conclusion, the urothelium glides over the lamina propria to fill wounds in an ERK-independent manner, whereas the epidermis crawls to cover wounds in an ERK-dependent manner.

Introduction

Collective cell migration is observed in many physiological and pathological processes such as development, epithelial wound healing, and cancer cell invasion[1-3]. In epithelial wound healing, monolayer or stratified layers of the epithelial cells migrate as a group and close the tissue defect over the underlying lamina propria[4-6]. Various physical and chemical cues induce front-to-rear polarity of cells at the free edge of a wound, referred to as leader cells, and their migration toward the free space[3, 6]. The leader cells transmit the polarity to the follower cells through mechanical coupling mediated by cell-cell junctions, and organize a movement in groups[7]. Moreover, diffusible molecules such as Ca^{2+}, H_2O_2, ATP, and growth factors also contribute by transmitting signals to the follower cells during the collective cell migration[8].

The molecular basis underlying the coordinated epithelial cell migration during wound healing has been extensively studied in vitro by using epithelial cell lines, including MDCK cells. For example, the Rho-family GTPases and extracellular signal-regulated kinase (ERK) have been shown to play roles in this migration process in MDCK cells[9, 10]. The classical scratch method to generate a wound in the monolayer MDCK cell sheet not only opens the space but also damages the cells, generating reactive oxygen species (ROS). It has been proposed that ROS at the wound edge are required for the activation of ERK and cell migration[11].

A new window into the study of the wound healing process has been opened by biosensors based on Förster resonance energy transfer (FRET)[12-14]. For instance, activation of Rho-family GTPases in the leader cells has been demonstrated by the time-lapse FRET imaging of wounded MDCK cell monolayers[15, 16]. More recently, we have discovered that repetitive waves of ERK activation were propagated away from the wound edge not only in MDCK cells but also in the ear skin of mice[17, 18]. Tidal waves of ERK activation were previously found to be propagated from the wound edge by immunohistochemistry[10, 11]; however, the repetitive waves of ERK activation from the wound edge[17] or spontaneous wavelets in the regions apart from the wound edge could only be visualized by time-lapse imaging of ERK activity with FRET biosensors[18]. Importantly, cells migrate against the direction of the ERK activation wave both in the mouse epidermis and in the MDCK

monolayer sheet[18].

A substantial part of our knowledge about wound healing *in vivo* comes from studies of epidermal wound healing, and the basic mechanism underlying wound healing is assumed to be conserved among different animals and tissues[5, 19]. Meanwhile, while there have been several studies on the wound healing of the urothelium[20-24], it remains elusive whether urothelial wounds are repaired in the same way as epidermal wounds. Recently, we performed *in vivo* imaging of the mouse urothelium by two-photon excitation microscopy (TPEM)[25]. During the course of the study, we noticed that the urothelium sometimes glides over the underlying lamina propria, and this observation urged us to examine the collective migration of the urothelium during wound healing. Here, we demonstrate that the collective migration of the urothelium is significantly different from that of the epidermis, not only in regard to the mode of migration but also in terms of the requirement for ERK activity.

Materials and Methods

Ethical Approval

The animal protocols were reviewed and approved by the Animal Care and Use Committee of Kyoto University Graduate School of Medicine (Nos. 12064, 13074, 14079, and 15064).

Animals

Transgenic mice expressing ERK FRET biosensors have been described previously[26]. ERK FRET biosensors, EKAREV-nuclear export signal (NES) and EKAREV-nuclear localization signal (NLS), are localized in the cytoplasm and the nucleus, respectively[26]. EKAREV-NES and EKAREV-NLS that were backcrossed more than five generations to C57BL/6N Jcl (CLEA Japan, Tokyo, Japan) were used for analysis. The Fucci mice, which express mAG-hGeminin (1/110) and mKO2-hCdt1 (30/120), were obtained from the Laboratory for Animal Resources and Genetic Engineering, RIKEN Center for Developmental Biology[27]. Mice were housed in a specific pathogen-free facility in temperature-controlled rooms with a 14-h light/10-h dark cycle and received a routine chow diet and water ad libitum. For intravital imaging of the skin and the bladder, 12- to 25-week-old mice were used. At the end of the

experiments, mice were euthanized by anesthetic overdose.

Two-photon excitation microscopy (TPEM)

We used an FV1000MPE-BX61WI upright microscope (Olympus, Tokyo, Japan) equipped with a 25×/1.05 water-immersion objective lens (XLPLN 25XWMP; Olympus), and an InSight DeepSee Ultrafast laser (0.95 W at 900 nm; Spectra Physics, Mountain View, CA). The excitation wavelength for cyan fluorescent protein (CFP) was 840 nm. An IR-cut filter, BA685RIF-3 (Olympus), two dichroic mirrors, DM505 and DM570 (Olympus), and four emission filters, FF01-425/30 (Semrock, Rochester, NY) for the second harmonic generation (SHG), BA460-500 (Olympus) for CFP, BA520-560 (Olympus) for yellow fluorescent protein (YFP), and 645/60 (Chroma Technology, Bellows Falls, VT) for Qtracker 655 (Life Technologies, Carlsbad, CA), were used. Qtracker 655 is intravenously administered with other reagents to confirm drug delivery to target organs. For Fucci mouse imaging, we used an IR-cut filter, RDM690 (Olympus), two dichroic mirrors, DM505 and DM570, and three emission filters, FF01-472/30 (Semrock) for SHG images, BA495-540 (Olympus) for mAG, and BA575-630 (Olympus) for mKO2. The microscope was equipped with a two-channel GaAsP detector unit and two built-in photomultiplier tubes. FluoView software (Olympus) was used to control the microscope and to acquire images, which were saved in the multilayer 16-bit tagged image file format.

Intravital imaging of mouse tissues

Intravital imaging of the bladder was performed as described previously[25]. Briefly, female mice were anesthetized by inhalation of 1-1.5% isoflurane (Abbott Laboratories, North Chicago, IL) and placed in the supine position on an electric heat pad maintained at 37 ºC. A 24-gauge ethylene tetrafluoroethylene catheter (Terumo, Tokyo, Japan) connected to a 50 mL bottle of normal saline (Otsuka Pharmaceutical Factory, Tokushima, Japan) was inserted transurethrally into the bladder. The intravesical pressure was controlled by the bottle's height and kept at 15-20 cm H_2O for 30 min. Then the catheter, which caused mechanical irritation and intensified the rhythmic muscle contraction of the bladder, was removed for stable long-

term imaging. The bladder was pulled out of the abdominal cavity and the bladder wall was immobilized on a custom-made vacuum-stabilized imaging window (Olympus). For multi-dimensional imaging of the urothelium and the underlying lamina propria, z-stack images were acquired using a 2.4 digital zoom at 0.5 μm intervals and at a scan speed of 8 μs/pixel. CFP, Qtracker 655 and SHG were imaged to show cells, blood vessels and collagen fibers, respectively. Time-lapse images were acquired every 5 or 6 min using a 1.2-2.4 digital zoom at a scan speed of 4 μs/pixel.

For the wound healing analysis of the urothelium, a square 100 μm on each side was set under the two-photo excitation microscope. After increasing the laser power to 80–100%, the area was repeatedly scanned until the CFP fluorescence signal became undetectable even with the highest sensitivity of the GaAsP detector.

Intravital imaging of the ear skin was performed as described previously[17]. Hairs were removed from an ear by using depilation cream 24 h before experiments. An ear of an anesthetized mouse was sandwiched between a cover glass and a thermal conductive silicon gum sheet. For multi-dimensional imaging of the epidermis and underlying lamina propria, z-stack images were acquired using a 3.0 digital zoom at 0.5 μm intervals and at a scan speed of 8 μs/pixel. Time-lapse images were acquired every 10 or 12 min. An epithelial wound was created at the ear skin with a 29 gauge needle (Terumo) 2 h before imaging.

PD0325901 (5 mg/kg), a mitogen-activated protein kinase/ERK kinase (MEK) inhibitor (EMD Millipore, Billerica, MA), was dissolved in 0.2 mL PBS supplemented with 4 μL Qtracker 655 and injected via the tail vein at a dose of 5 mg/kg. Dasatinib, a tyrosine kinase inhibitor (AdooQ BioScience, Irvine, CA), was dissolved in 0.15 mL propylene glycol supplemented with 4 μL Qtracker 655 and injected via the tail vein at a dose of 10 mg/kg.

Image processing

Microscopic images were analyzed as described previously with MetaMorph software (version 7.10.1.161; Molecular Devices, Sunnyvale, CA)[28]. In brief, YFP fluorescence images obtained by the excitation of CFP were used as FRET images. The FRET level is evaluated by the FRET/CFP ratio and represented as an intensity-modulated display (IMD) or golden

pseudocolor images. In the IMD mode, 8 colors from red to blue represent the FRET/CFP ratio, and the 32 grades of intensity represent the signal intensity in each pixel of the CFP image. The warm and cold colors were assigned to high and low FRET levels, respectively. The FRET/CFP ratio of each cell was quantified as follows. For the biosensor located in the nucleus, a region of interest (ROI) was created to include each nucleus. For the biosensor located in the cytoplasm, nuclear signals was first subtracted by the H-basin filter of MetaMorph. By using auto-threshold, a ROI was set onto the cytoplasm. Then, the region was expanded 3 pixels outward. The average fluorescence intensity of the ROI was used to calculate the FRET/CFP ratio of each cell.

Cell cycle analysis was performed with Fucci mice according to the method reported previously[17]. The Fucci biosensor system consisted of two fluorescence reporters, the mKO2-hCdt1 (30/120) G1 marker and mAG-hGeminin (1/110) S/G2M marker, which emanate orange and green colors, respectively. For the identification of the nuclei of S/G2/M cells, images of mKO2-hCdt1 (30/120) were subtracted from images of mAG-hGeminin (1/110). The resulting images were processed with the segmentation function of the multi-dimensional motion analysis module of MetaMorph. The parameters used for the segmentation were: segmentation method, adaptive threshold; XY diameter, 4–20; local intensity above background, 100. The nuclei of G0/G1 cells were identified in a similar manner.

To track cell migration, the FRET images were analyzed by using the Fiji TrackMate plugin[29, 30]. The tracking data were further processed by the Chemotaxis & Migration Tool (version 1.01; ibidi GmbH, Martinsried, Germany).

Statistical analysis

All statistical analyses were performed using Prism5 software (version 6; GraphPad Software, La Jolla, CA). A paired Student's *t*-test was used to evaluate statistically significant differences. P values < 0.05 were considered statistically significant and are shown in the figures.

Results

Time-lapse imaging of the urothelium, the epidermis, and the underlying lamina propria

Both skin and bladder are covered by stratified epithelium. We first show the remarkable difference between these two epithelia in the mobility over the underlying lamina propria. For this observation, we used two transgenic mouse lines expressing a nuclear FRET biosensor for ERK, EKAREV-NLS (nuclear localization signal), or a cytoplasmic FRET biosensor for ERK, EKAREV-NES (nuclear export signal)[25, 26]. Both the epidermis and the urothelium are supported by dense collagen fibers in the lamina propria (Figure 1A-D). A peculiar anatomical feature of the bladder is the presence of suburothelial capillary plexus and interstitial cells beneath the urothelium (Figure 1B and D). During the 2 h observation of mice expressing EKAREV-NLS, the nuclei of epidermal basal cells did not move significantly (Figure 1E left and 1F left, Supplemental Video S1). In stark contrast, the nuclei of urothelial cells were frequently moving (Figure 1E right and 1F right, Supplemental Video S1). Consequently, the displacement during the 1 h imaging was larger in the urothelium than the epidermis (Figure 1G). Notably, we occasionally observed that the urothelial cell sheet glided over the suburothelial capillary plexus (Figure 1H, Supplemental Video S2). These observations may suggest that the adhesion to the underlying lamina propria appears markedly weaker in the urothelium than the epidermis. Of note, we did not find significant difference in the mobility between the basal layer cells and the umbrella cells.

Difference in the mode of collective cell migration during wound healing between the epidermis and the urothelium

The seemingly loose adhesion of the urothelium to the underlying lamina propria prompted us to examine the mode of collective cell migration. For this examination, we observed the epidermis and the urothelium during wound healing by TPEM. In the skin, a microscopic injury of 150-300 μm diameter was generated with a fine needle, followed by time-lapse imaging (Figure 2A, Supplementary Video S3). Cells were tracked by the TrackMate add-in program in Fiji to calculate their mean velocity and distance from the wound center (Figure 2B and C). Epidermal cells of two to three rows from the wound edge rapidly migrated

toward the wound center, whereas cells behind the front rows migrated rather slowly. This observation agrees with the previously reported results of an in vitro wound healing assay with MDCK cells[31]. FRET/CFP ratio videos were generated to analyze the dynamics of ERK activity. As we reported earlier[17, 18], ERK activation waves were propagated from the wound edge, as seen in Supplementary Video S3.

Similar experiments were set up for the urothelium, although the imaging period of the urothelium could not be as long as that of the ear skin due to the invasiveness of the imaging procedure. Because we failed to generate a mechanical wound with a fine needle through the urethral catheter, we applied intensive laser radiation to thermally ablate the urothelium. For this, a square 100 μm on each side was set on the urothelium and scanned repeatedly under the microscope with 80-100% laser power until the fluorescence disappeared completely. In this condition, we did not detect tissue damage of the lamina propria (Supplementary Figure). The wound healing process was initiated soon after the laser ablation (Figure 2D-F; Supplementary Video S4). In contrast to the epidermal cells, all urothelial cells within the imaged area glided at similar speeds to fill the defect, indicating that the mode of wound healing is significantly different between the epidermis and the urothelium. In addition, an ERK activation wave was not generated or propagated from the wound edge, suggesting that the biochemical mechanism underlying the cell migration may also be different between the epidermis and the urothelium. The experiments were repeated three times to confirm our observations (Figure 2F). Although the velocity of collective migration changed slightly in each experiment, the mode of collective migration did not change.

Requirement of ERK for the collective cell migration of the epidermis but not the urothelium

Next, to examine the role of ERK activation in collective cell migration, the MEK inhibitor PD0325901 was intravenously administered during time-lapse imaging. By the immunoblotting of the tissue samples, we previously confirmed that ERK phosphorylation is markedly suppressed under this condition[25]. ERK activity and the migration velocity of cells within 20 μm of the wound edge were quantitated before and after the inhibitor administration

(Figure 3A-D). In the wounded epidermis, both the basal activity in each cell and the propagation of activation waves of ERK were suppressed by the MEK inhibitor (Figure 3A and C). Epidermal cell migration was also significantly inhibited, albeit not completely, suggesting the requirement of ERK activity for migration (Figure 3D). In the urothelium as well, PD0325901 inhibited ERK activity (Figure 3B and C). However, the migration velocity of urothelial cells was not decreased to a statistically significant level, indicating that the ERK activity was dispensable for the gliding migration of the urothelium (Figure 3D).

The Fak-Src-ERK signaling pathway is known to play a pivotal role in the activation and inactivation of integrins at focal contact[32]. The modest effect of ERK inhibition on the gliding migration of urothelium might suggest that the urothelial cells migrate without disanchoring of the integrin from the underlying matrix. In other words, the urothelium may fill the gap by passive gliding over the lamina propria. To test this hypothesis, we examined the effect of the src inhibitor dasatinib. The effect of dasatinib on ERK was modest in the epidermis and not significant in the urothelium (Figure 3E). Nevertheless, dasatinib decreased the velocity of not only the epidermis but also the urothelium (Figure 3F). Thus, the urothelial migration, as well as the epidermal migration, requires the activation/inactivation cycle of integrin-mediated binding to the substrate. This observation also suggests that the urothelial gliding during the wound healing is not a passive movement, but an active tyrosine kinase-dependent cell migration.

Induction of cell proliferation in the epidermis but not the urothelium

Finally, we examined whether cell proliferation may have any roles in the collective migration of the epidermis and urothelium. For this purpose, we visualized the cell cycle by the use of Fucci mice, in which G1 cells could be discriminated from S/G2/M cells[27]. To use the same method for the wounding, both the epidermis and the urothelium were ablated in this experiment. Although it took a few hours until the epidermal cells started moving after the laser ablation, collective cell migration was clearly observed. As shown in Figure 4, less than 10% of basal epidermal cells were in S/G2/M phase before wounding. Six hours after laser ablation, the proportion of S/G2/M cells increased significantly in the regions close to the

wound edge, but not in the other regions. In the urothelium, S/G2/M cells were very rare, which is consistent with the previous report demonstrating a slow turnover rate (>3 months)[33]. Importantly, even after laser ablation, we failed to see any increase in the proportion of S/G2/M cells. These results strongly suggested that cell proliferation in the epithelium close to the wound may contribute to closing the wound in the epidermis, but not the urothelium, during the time scale of our observation. The urothelial cells that entered into S/G2/M phase might be scatted widely in the urothelium outside the viewfield.

Discussion

For a long period, the urothelium was believed to be pseudostratified and structurally different from the epidermis; i.e., all urothelial cells were thought to be more or less connected to the basement membrane[34]. However, it has been demonstrated that umbrella cells at the apical surface do not have connection to the basement membrane, indicating that the urothelium is a true stratified epithelium like the epidermis[35]. In this study, *in vivo* time-lapse imaging clearly demonstrated that the urothelium is more mobile than the epidermis and occasionally glides over the underlying lamina propria, highlighting the significant difference in mobility between the epidermis and the urothelium (Figure 1). This high mobility of the urothelium over the underlying lamina propria was more clearly demonstrated in the collective cell migration during the wound healing process (Figure 2). We can reasonably speculate that such high mobility, or gliding ability, assists in allowing the urothelium to adapt to the changes in the surface area during the micturition cycle.

It should be emphasized that the gliding of the urothelium over the underlying lamina propria could only be discovered by *in vivo* time-lapse imaging. To the best of our knowledge, previous observations of the urothelium by TPEM used ex vivo samples[36-38]. Optimal migration of lymphocytes in explanted lymph nodes requires a high concentration of oxygen[39, 40]. Therefore, the lack of blood flow and resulting low tissue oxygen concentration under the previous experimental conditions might have concealed the gliding of the urothelium. We cannot exclude the possibility that our experimental conditions including anesthesia also affected the mobility of the urothelium. At least, the blood flow remained

309 normal under our experimental conditions[25], suggesting that our model seems to replicate the
310 physiological conditions in terms of oxygen concentration. Another concern about the *in vivo*
311 imaging of the bladder is the application of hydrostatic pressure. Currently, we could observe
312 the bladder from the serosa as deep as 350 μm by TPEM. For the acquisition of urothelial
313 images, at least 14 cm hydrostatic pressure has to be applied to extend the muscle layer.
314 Therefore, the mode of urothelial cell migration may be different in the bladder at lower
315 intravesical pressure. Last, the epidermis and the urothelium were abraded by needle injection
316 and laser ablation, respectively, to observe the collective cell migration (Figure 2). This is
317 because, in preliminary experiments, the epidermal cells migrated only slowly after the laser
318 ablation, which prevented us from quantitative analysis during the 12 h time-lapse imaging.
319 Therefore, the difference in the method used to abrade the epithelium might have affected the
320 difference in the mode of migration.

321 Urothelial cells bind to the basement membrane via hemidesmosomes as do epidermal
322 cells[41-43]. Hemidesmosomes are comprised of several proteins, among which integrin-family
323 proteins play critical roles to anchor the cells to the basement membrane[44]. In tissue culture
324 cells, focal adhesions provide the loci for integrin-mediated cell-to-substrate anchoring and
325 ERK activity is required for the turnover of the focal adhesions[45, 46]. Taking these previous
326 reports into consideration, the dispensability of ERK for the urothelial migration may suggest
327 the high fluidity of the lamina propria. In other words, the urothelium may be connected only
328 loosely to the underlying lamina propria. However, against this hypothesis, dasatinib, the Src
329 inhibitor, inhibited the urothelial migration (Figure 3F), indicating that the migration of the
330 urothelium is an active process that requires the activation of tyrosine kinases.

331 In MDCK cells, the ERK activation wave is propagated from the leader cells to promote
332 collective cell migration[10, 31]. Importantly, the cell density and the ERK activity are inversely
333 correlated[18]. Therefore, the MDCK cell sheet crawls over the substrate with the cycle of
334 shrinkage and extension of each cell. We speculate that the epidermal cells migrate in a
335 manner similar to MDCK cells (Fig. 5). In contrast, the urothelium appears to glide over the
336 lamina propria more smoothly without significant changes in size (Fig. 5). This observation
337 may explain the dispensability of ERK activity for the collective cell migration of the

urothelium. It should also be noted that inhibitors for the Ras-ERK MAP kinase pathway are now clinically approved for some cancers such as melanoma[47]. Inhibitors against MEK and BRAF are known to perturb the wound healing of the epidermis[48], but little is known about the wound healing of the urothelium. Our observations imply that the inhibitors for the Ras-ERK MAP kinase pathway are less toxic to the urothelium than the epidermis because of the difference in the mode of migration.

In conclusion, *in vivo* time-lapse imaging of the wound healing process highlighted a marked difference in the mode of the collective cell migration between the epidermis and the urothelium. *In vivo* TPEM was effective for observing the dynamic nature of cell movement and molecular activities, and its use in these contexts will shed new light on the experimental pathology of wounds.

Acknowledgements

We are grateful to the members of the Matsuda Laboratory for their helpful input, to Kyoko Hirano, Kanako Takakura, Nobuyo Sakikawa, and Akiko Kawagishi for their technical assistance, and to the Medical Research Support Center of Kyoto University for *in vivo* imaging.

T.S., T.K., O.O., and M.M. conceived the experiments; T.S. performed the experiments; T.S. and M.M. analyzed the data; T.S., T.K., and M.M. wrote the manuscript.

References

1. Rorth P: Collective cell migration, Annu Rev Cell Dev Biol 2009, 25:407-429
2. Weijer CJ: Collective cell migration in development, J Cell Sci 2009, 122:3215-3223
3. Haeger A, Wolf K, Zegers MM, Friedl P: Collective cell migration: guidance principles and hierarchies, Trends Cell Biol 2015, 25:556-566
4. Martin P: Wound healing--aiming for perfect skin regeneration, Science 1997, 276:75-81
5. Sonnemann KJ, Bement WM: Wound repair: toward understanding and integration of single-cell and multicellular wound responses, Annu Rev Cell Dev Biol 2011, 27:237-263
6. Shaw TJ, Martin P: Wound repair: a showcase for cell plasticity and migration, Curr Opin Cell Biol 2016, 42:29-37
7. Ladoux B, Mege RM, Trepat X: Front-rear polarization by mechanical cues: From single cells to tissues, Trends Cell Biol 2016, 26:420-433
8. Cordeiro JV, Jacinto A: The role of transcription-independent damage signals in the initiation of epithelial wound healing, Nat Rev Mol Cell Biol 2013, 14:249-262
9. Fenteany G, Janmey PA, Stossel TP: Signaling pathways and cell mechanics involved in wound closure by epithelial cell sheets, Curr Biol 2000, 10:831-838
10. Matsubayashi Y, Ebisuya M, Honjoh S, Nishida E: ERK activation propagates in epithelial cell sheets and regulates their migration during wound healing, Curr Biol 2004, 14:731-735
11. Nikolic DL, Boettiger AN, Bar-Sagi D, Carbeck JD, Shvartsman SY: Role of boundary conditions in an experimental model of epithelial wound healing, Am J Physiol Cell Physiol 2006, 291:C68-75
12. Aoki K, Kamioka Y, Matsuda M: Fluorescence resonance energy transfer imaging of cell signaling from in vitro to in vivo: Basis of biosensor construction, live imaging, and image processing, Dev Growth Differ 2013, 55:515-522
13. Oldach L, Zhang J: Genetically encoded fluorescent biosensors for live-cell visualization of protein phosphorylation, Chem Biol 2014, 21:186-197
14. Enterina JR, Wu L, Campbell RE: Emerging fluorescent protein technologies, Curr Opin Chem Biol 2015, 27:10-17

15. Kurokawa K, Matsuda M: Localized RhoA activation as a requirement for the induction of membrane ruffling, Mol Biol Cell 2005, 16:4294-4303
16. Reffay M, Parrini MC, Cochet-Escartin O, Ladoux B, Buguin A, Coscoy S, Amblard F, Camonis J, Silberzan P: Interplay of RhoA and mechanical forces in collective cell migration driven by leader cells, Nat Cell Biol 2014, 16:217-223
17. Hiratsuka T, Fujita Y, Naoki H, Aoki K, Kamioka Y, Matsuda M: Intercellular propagation of extracellular signal-regulated kinase activation revealed by in vivo imaging of mouse skin, eLife 2015, 4:e05178
18. Aoki K, Kondo Y, Naoki H, Hiratsuka T, Itoh RE, Matsuda M: Propagating wave of ERK activation orients collective cell migration., Dev Cell 2017, 43:305-317
19. Gurtner GC, Werner S, Barrandon Y, Longaker MT: Wound repair and regeneration, Nature (London) 2008, 453:314-321
20. Dalal E, Medalia O, Harari O, Aronson M: Moderate stress protects female mice against bacterial infection of the bladder by eliciting uroepithelial shedding, Infect Immun 1994, 62:5505-5510
21. Veranic P, Jezernik K: The response of junctional complexes to induced desquamation in mouse bladder urothelium, Biol Cell 2000, 92:105-113
22. Apodaca G, Kiss S, Ruiz W, Meyers S, Zeidel M, Birder L: Disruption of bladder epithelium barrier function after spinal cord injury, Am J Physiol Renal Physiol 2003, 284:F966-976
23. Andreoni CR, Lin HK, Olweny E, Landman J, Lee D, Bostwick D, Clayman RV: Comprehensive evaluation of ureteral healing after electrosurgical endopyelotomy in a porcine model: original report and review of the literature, J Urol 2004, 171:859-869
24. Kreft ME, Sterle M, Veranic P, Jezernik K: Urothelial injuries and the early wound healing response: tight junctions and urothelial cytodifferentiation, Histochem Cell Biol 2005, 123:529-539
25. Sano T, Kobayashi T, Negoro H, Sengiku A, Hiratsuka T, Kamioka Y, Liou LS, Ogawa O, Matsuda M: Intravital imaging of mouse urothelium reveals activation of extracellular signal-regulated kinase by stretch-induced intravesical release of ATP, Physiol Rep 2016,

4:

26. Kamioka Y, Sumiyama K, Mizuno R, Sakai Y, Hirata E, Kiyokawa E, Matsuda M: Live imaging of protein kinase activities in transgenic mice expressing FRET biosensors, Cell Struct Funct 2012, 37:65-73
27. Sakaue-Sawano A, Kurokawa H, Morimura T, Hanyu A, Hama H, Osawa H, Kashiwagi S, Fukami K, Miyata T, Miyoshi H, Imamura T, Ogawa M, Masai H, Miyawaki A: Visualizing spatiotemporal dynamics of multicellular cell-cycle progression, Cell 2008, 132:487-498
28. Mizuno R, Kamioka Y, Kabashima K, Imajo M, Sumiyama K, Nakasho E, Ito T, Hamazaki Y, Okuchi Y, Sakai Y, Kiyokawa E, Matsuda M: In vivo imaging reveals PKA regulation of ERK activity during neutrophil recruitment to inflamed intestines, J Exp Med 2014, 211:1123-1136
29. Jaqaman K, Loerke D, Mettlen M, Kuwata H, Grinstein S, Schmid SL, Danuser G: Robust single-particle tracking in live-cell time-lapse sequences, Nat Methods 2008, 5:695-702
30. Applegate KT, Besson S, Matov A, Bagonis MH, Jaqaman K, Danuser G: plusTipTracker: Quantitative image analysis software for the measurement of microtubule dynamics, J Struct Biol 2011, 176:168-184
31. Farooqui R, Fenteany G: Multiple rows of cells behind an epithelial wound edge extend cryptic lamellipodia to collectively drive cell-sheet movement, J Cell Sci 2005, 118:51-63
32. Kleinschmidt EG, Schlaepfer DD: Focal adhesion kinase signaling in unexpected places, Curr Opin Cell Biol 2017, 45:24-30
33. Jost SP: Cell cycle of normal bladder urothelium in developing and adult mice, Virchows Arch B Cell Pathol Incl Mol Pathol 1989, 57:27-36
34. Tanaka K: Polarisationsoptische Analyse der Übergangsepithelien des Menschen, Arch Histol Jpn 1962, 22:229-236
35. Jost SP, Gosling JA, Dixon JS: The morphology of normal human bladder urothelium, J Anat 1989, 167:103-115
36. Zhuo SM, Chen JX, Luo T, Jiang XS, Xie SS: Multiphoton microscopy of unstained

445 bladder mucosa based on two-photon excited autofluorescence and second harmonic
446 generation, Laser Physics Letters 2009, 6:80-83
447 37. Xu J, Kang D, Xu M, Zhuo S, Zhu X, Chen J: Multiphoton microscopic imaging of
448 esophagus during the early phase of tumor progression, Scanning 2013,
449 38. Schueth A, van Zandvoort MA, Buurman WA, van Koeveringe GA: Murine Bladder
450 Imaging by 2-Photon Microscopy: An Experimental Study of Morphology, J Urol 2014,
451 39. Miller MJ, Wei SH, Parker I, Cahalan MD: Two-Photon Imaging of Lymphocyte Motility
452 and Antigen Response in Intact Lymph Node, Science 2002, 296:1869
453 40. Huang JH, Cárdenas-Navia LI, Caldwell CC, Plumb TJ, Radu CG, Rocha PN, Wilder T,
454 Bromberg JS, Cronstein BN, Sitkovsky M, Dewhirst MW, Dustin ML: Requirements for
455 T Lymphocyte Migration in Explanted Lymph Nodes, J Immunol 2007, 178:7747
456 41. Alroy J, Gould VE: Epithelial-stromal interface in normal and neoplastic human bladder
457 epithelium, Ultrastruct Pathol 1980, 1:201-210
458 42. Woldemeskel M, Drommer W, Wendt M: Histology and ultrastructure of the urothelium
459 lining the ureter and the renal pelvis in sows, Anat Histol Embryol 1998, 27:51-55
460 43. Owaribe K, Kartenbeck J, Stumpp S, Magin TM, Krieg T, Diaz LA, Franke WW: The
461 hemidesmosomal plaque. I. Characterization of a major constituent protein as a
462 differentiation marker for certain forms of epithelia, Differentiation 1990, 45:207-220
463 44. Parsons JT, Horwitz AR, Schwartz MA: Cell adhesion: integrating cytoskeletal dynamics
464 and cellular tension, Nat Rev Mol Cell Biol 2010, 11:633-643
465 45. Xie H, Pallero MA, Gupta K, Chang P, Ware MF, Witke W, Kwiatkowski DJ,
466 Lauffenburger DA, Murphy-Ullrich JE, Wells A: EGF receptor regulation of cell motility:
467 EGF induces disassembly of focal adhesions independently of the motility-associated
468 PLCγ signaling pathway, J Cell Sci 1998, 111 (Pt 5):615-624
469 46. Fincham VJ, James M, Frame MC, Winder SJ: Active ERK/MAP kinase is targeted to
470 newly forming cell-matrix adhesions by integrin engagement and v-Src, EMBO J 2000,
471 19:2911-2923
472 47. Simanshu DK, Nissley DV, McCormick F: RAS Proteins and Their Regulators in Human
473 Disease, Cell 2017, 170:17-33

474 48. Escuin-Ordinas H, Li S, Xie MW, Sun L, Hugo W, Huang RR, Jiao J, de-Faria FM,
475 Realegeno S, Krystofinski P, Azhdam A, Komenan SMD, Atefi M, Comin-Anduix B,
476 Pellegrini M, Cochran AJ, Modlin RL, Herschman HR, Lo RS, McBride WH, Segura T,
477 Ribas A: Cutaneous wound healing through paradoxical MAPK activation by BRAF
478 inhibitors, Nat Commun 2016, 7:12348

Figure Legends

Figure 1. Gliding of the urothelium over the lamina propria. A-D: Merged images of FRET (gray scale), SHG (green) and Qtracker 655 (red) by multi-photon imaging of the mouse ear skin and bladder wall expressing EKAREV-NLS (A and B) and EKAREV-NES (C and D). In panel D, the upper left quarter of SHG of the suburothelium is removed to show the interstitial cells more clearly. E and F: Motion analysis (E) and trajectory analysis (F) of the epidermis and the urothelium (Supplementary Video S1) of an EKAREV-NLS mouse. FRET images acquired every 20 min are superimposed and four colors are assigned according to the time points of image acquisition as indicated by the color bar (E). The scale bars represent 50 μm (A-E). Displacement of the centroid of the nuclei during the 1 h imaging is shown on X-Y planes (N>1000 and N>100 in the epidermis and the urothelium, respectively) (F). The yellow crosses indicate the averages. G: Bee-swarm plots of the displacement of the nuclei for all cells (left) and averages (right). Red brackets and red lines are means and standard deviations, respectively. H: A superimposition of 30 time-series FRET images at the interface between the urothelium and the lamina propria. Seven colors are assigned according to the time points of image acquisition as indicated by the color bar. All images were superimposed to show that the urothelial cells moved from left to right as the time elapsed. The elliptical nuclei of the interstitial cells (yellow arrows) and the elongated nuclei of the endothelial cells (white arrowheads) are white, indicating that these cells stayed in the same position during the imaging (see Supplementary Video S2). The right panels show a schematic diagram of the urothelium gliding over the lamina propria. The scale bar represents 20 μm. The red arrows in the right panel illustrate the track of basal cells gliding over the lamina propria.

Figure 2. Distinct mode of collective cell migration between the epidermis and urothelium. A: An epithelial wound was created on the ear skin of each transgenic mouse expressing EKAREV-NES. Two hours after wounding, the mice were observed under TPEM for 12 h. CFP and FRET images were acquired every 10 min to generate video of FRET/CFP ratio images (Video 3). Shown here are the FRET image and FRET/CFP ratio image in intensity modulated display mode with the ratio range shown on the right. Scale bars = 100 μm. B:

Tracks and the velocities of the epidermal cells were generated as described in the text. C: Cells that could be tracked for at least 7 sequential time-lapse images were analyzed to plot the distance from the center of the wound and mean velocity. $n = 3$. D: Transgenic mice expressing EKAREV-NES were subjected to observation. Under a two-photon excitation microscope, a urothelial wound was created by laser ablation. Images were acquired every 6 min for 8 h (Video 4). FRET and FRET/CFP ratio images are shown. Scale bars = 100 μm. E: Tracks and the velocities of the epidermal cells were generated as described in the text. F: Cells that could be tracked for at least 6 sequential time-lapse images were analyzed to plot the distance from the center of the wound and mean velocity. $n = 3$. The black, cyan, and red dots in panels C and F indicate datasets from three independent experiments.

Figure 3. Differential sensitivity to an MEK inhibitor between the wound healing of the epidermis and urothelium. A, B: An epithelial wound or a urothelial wound was created in each transgenic mouse expressing EKAREV-NES. Two hours after wounding, the mice were observed by TPEM for at least 3 h. CFP and FRET images were acquired to generate FRET/CFP ratio images. The MEK inhibitor PD0325901 (5 mg/kg) was intravenously injected 1 h after the start of image acquisition. Representative FRET/CFP ratio images before and after the administration of the MEK inhibitor are shown. Scale bars = 100 μm. C: Shown here are the mean ERK activity (FRET/CFP) of three mice at time zero (pre) and 1 h (post). D: Leader cells within 20 μm of the wound edge were subjected to trajectory analysis to calculate the mean velocity of migration. E, F: Similar experiments were performed except that the tyrosine kinase inhibitor Dasatinib (10 mg/kg) was administrated at time zero. Three mice were used for each condition. $*P < 0.05$, $**P < 0.01$, $***P < 0.001$.

Figure 4. Cell cycle progression in the epidermis but not the urothelium after injury. A: An epithelial wound or a urothelial wound was created in each transgenic mouse expressing Fucci, a genetically-encoded sensor for the cell-cycle. The mice were observed by TPEM for 12 h. The Fucci biosensor system consisted of an mAG-hGeminin (green) S/G2/M marker and an mKO2-hCdt1 (red) G1 marker. Scale bars = 50 μm. B: The percentages of

S/G2/M cells in the leader cells, within 20 μm of the wound edge, and the other follower cells were scored and plotted. The number of S/G2/M cells in the urothelium was negligible during the observation.

Figure 5. Schematic view of the crawling migration of the epidermis and the gliding migration of the urothelium during the wound healing. In the epidermis, the ERK activation wave is accompanied by a decrease in cell density, which drives the cell sheet to crawl over the underlying lamina propria. In contrast, the urothelium glides over the lamina propria without the waves of ERK activation and cell density change.

Figure 1

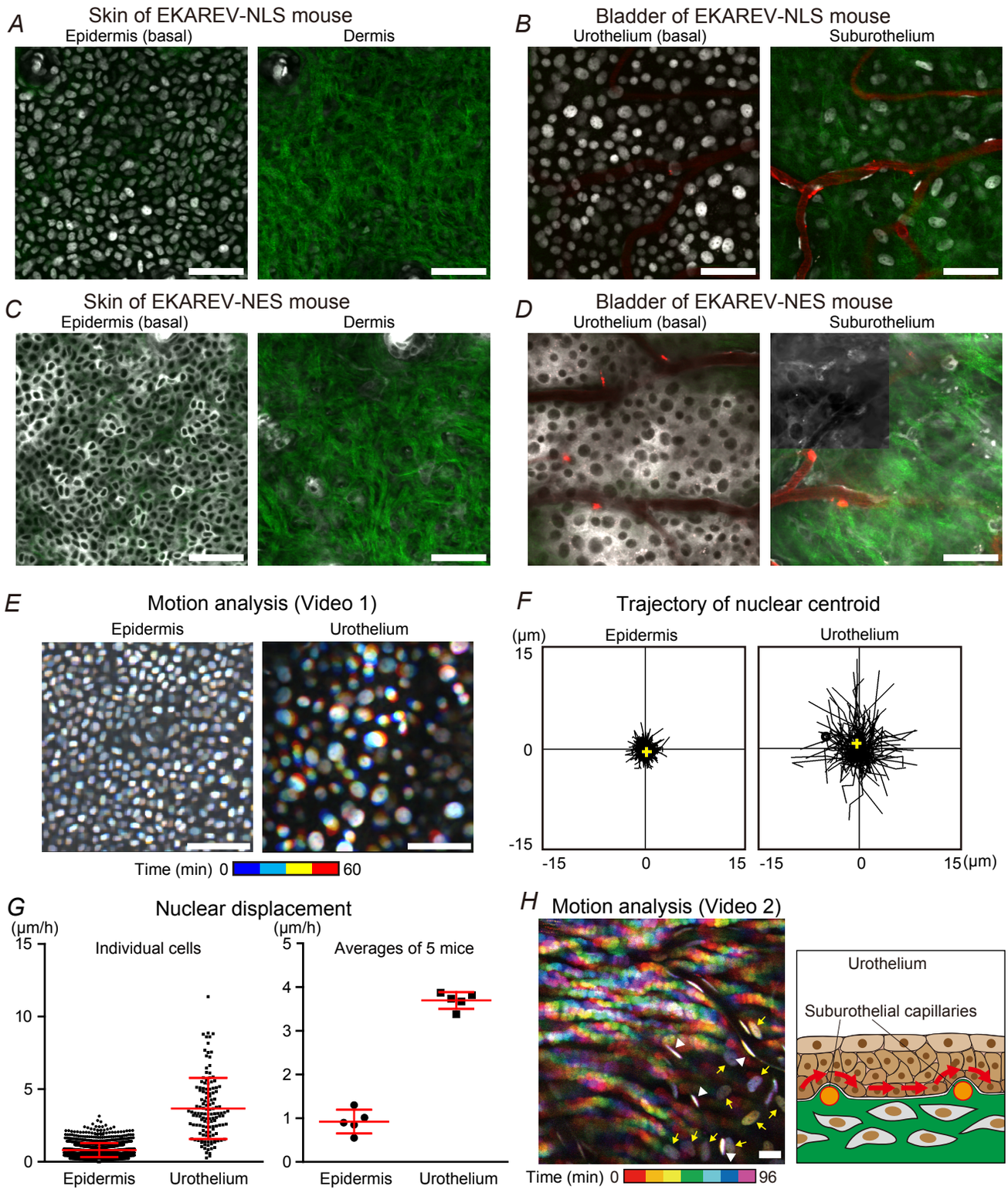
A
Skin of EKAREV-NLS mouse
Epidermis (basal)
Dermis
B
Bladder of EKAREV-NLS mouse
Urothelium (basal)
Suburothelium
C
Skin of EKAREV-NES mouse
Epidermis (basal)
Dermis
D
Bladder of EKAREV-NES mouse
Urothelium (basal)
Suburothelium
E
Motion analysis (Video 1)
Epidermis
Urothelium
Time (min) 0
60
F
Trajectory of nuclear centroid
(μm)
Epidermis
Urothelium
15
0
-15
-15
0
15
-15
0
15 (μm)
G
Nuclear displacement
(μm/h)
Individual cells
(μm/h)
Averages of 5 mice
15
10
5
0
5
4
3
2
1
0
Epidermis
Urothelium
Epidermis
Urothelium
H
Motion analysis (Video 2)
Time (min) 0
96
Urothelium
Suburothelial capillaries

Figure 2

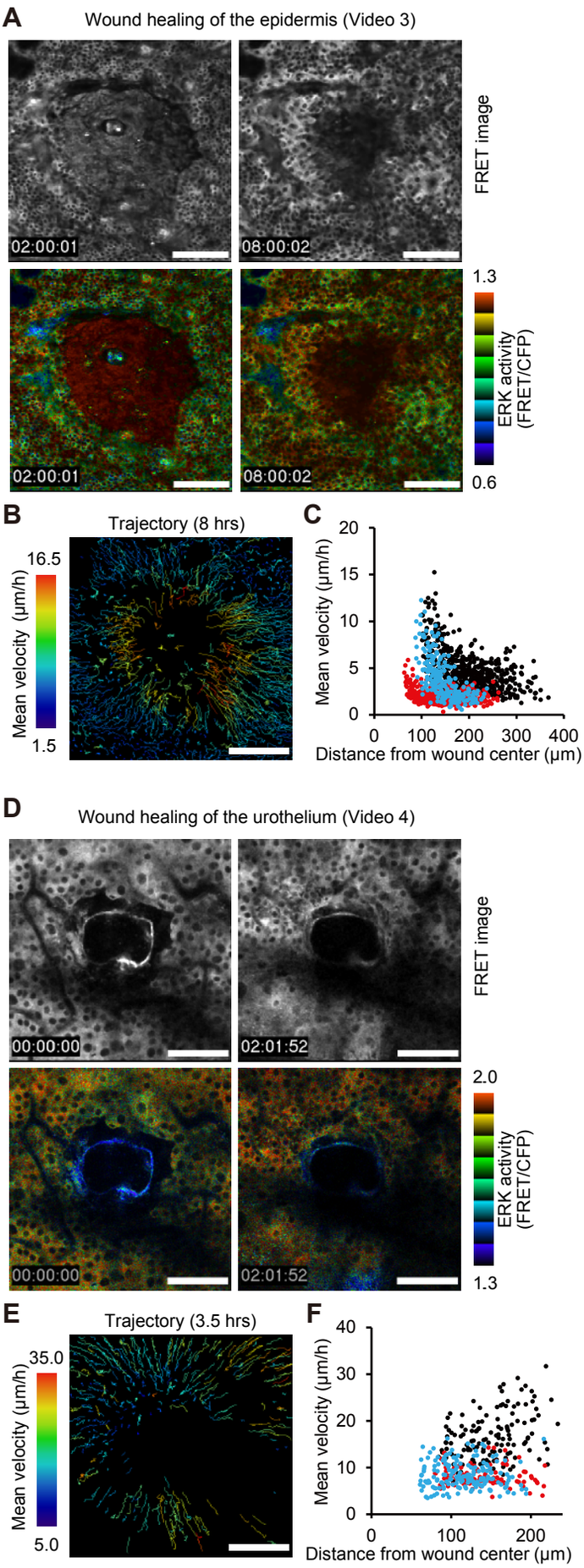
A
Wound healing of the epidermis (Video 3)
02:00:01
08:00:02
FRET image
1.3
ERK activity (FRET/CFP)
0.6
B
Trajectory (8 hrs)
16.5
Mean velocity (μm/h)
1.5
C
Mean velocity (μm/h)
Distance from wound center (μm)
D
Wound healing of the urothelium (Video 4)
00:00:00
02:01:52
2.0
1.3
E
Trajectory (3.5 hrs)
35.0
5.0
F

Figure 3

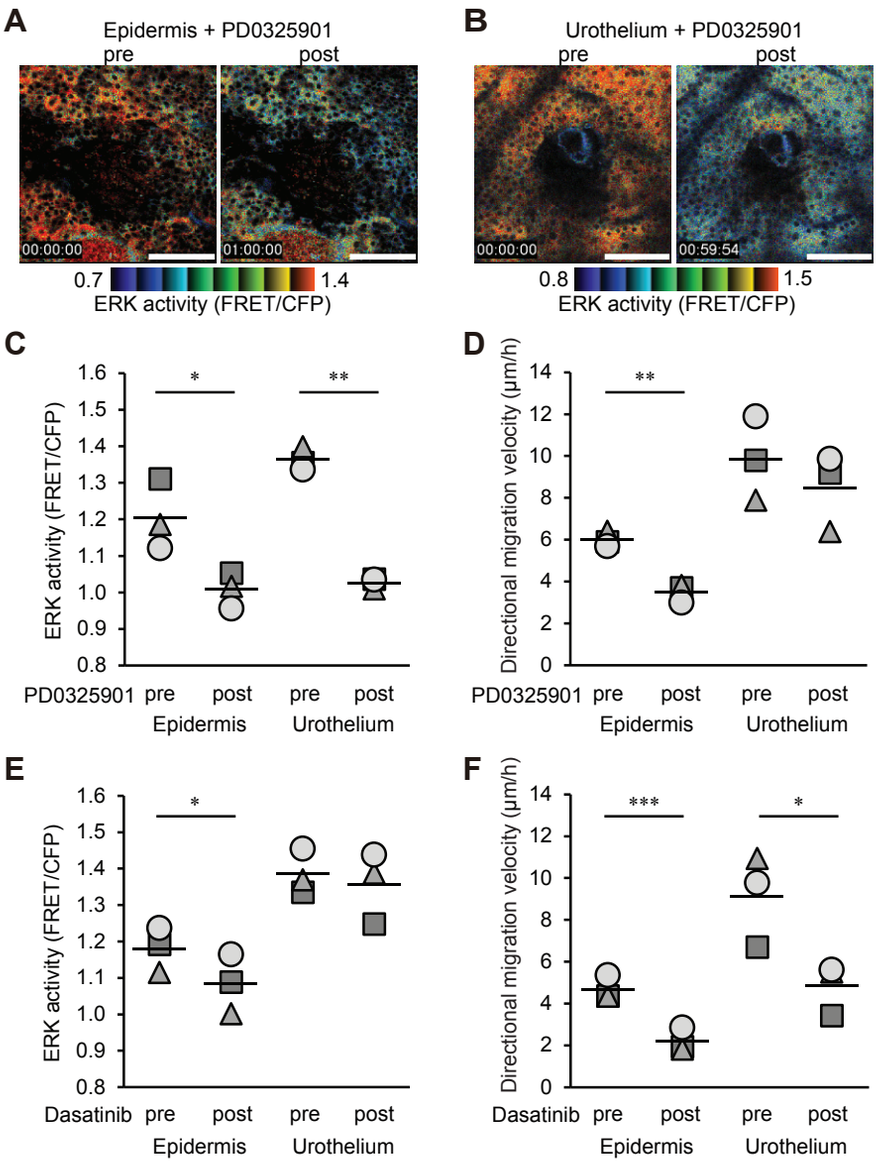
A
Epidermis + PD0325901
pre
post
00:00:00
01:00:00
0.7
1.4
ERK activity (FRET/CFP)
B
Urothelium + PD0325901
pre
post
00:00:00
00:59:54
0.8
1.5
ERK activity (FRET/CFP)
C
ERK activity (FRET/CFP)
PD0325901 pre post pre post
Epidermis
Urothelium
D
Directional migration velocity (μm/h)
PD0325901 pre post pre post
Epidermis
Urothelium
E
ERK activity (FRET/CFP)
Dasatinib pre post pre post
Epidermis
Urothelium
F
Directional migration velocity (μm/h)
Dasatinib pre post pre post
Epidermis
Urothelium

Figure 4

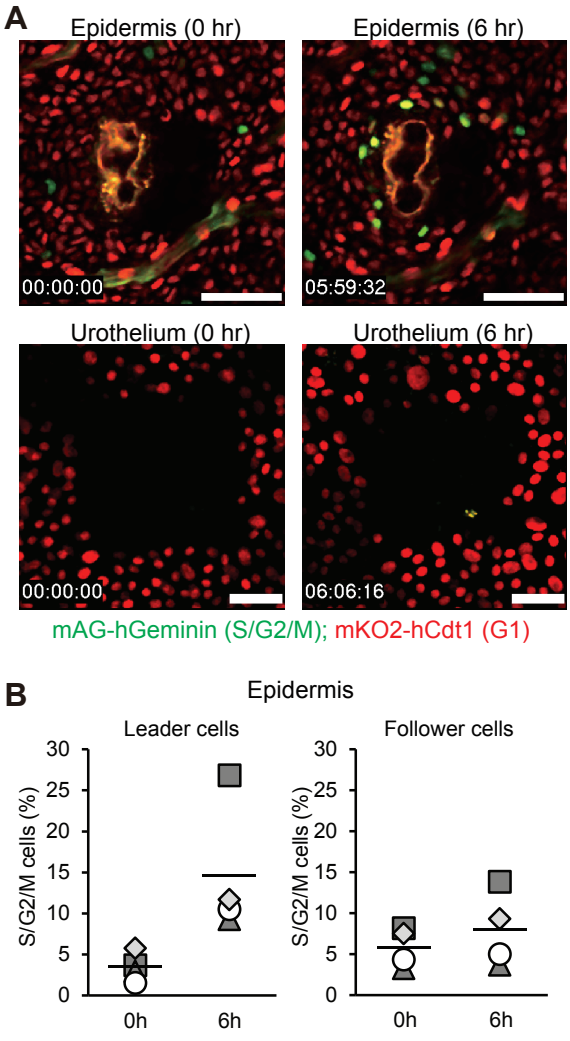
A
Epidermis (0 hr)
Epidermis (6 hr)
00:00:00
05:59:32
Urothelium (0 hr)
Urothelium (6 hr)
00:00:00
06:06:16
mAG-hGeminin (S/G2/M); mKO2-hCdt1 (G1)
B
Epidermis
Leader cells
Follower cells
S/G2/M cells (%)
30
25
20
15
10
5
0
0h
6h

Figure 5

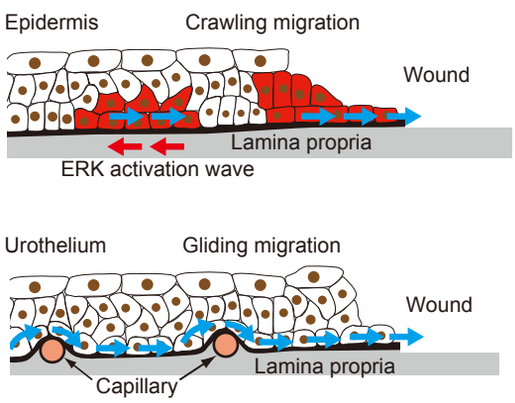
Epidermis
Crawling migration
Wound
Lamina propria
ERK activation wave
Urothelium
Gliding migration
Wound
Lamina propria
Capillary

Supplemental Figure